EXTREME LANDFALLING ATMOSPHERIC RIVER EVENTS IN ARIZONA: POSSIBLE FUTURE CHANGES

BY

ITINDERJOT SINGH

THESIS

Submitted in partial fulfillment of the requirements
for the degree of Master of Science in Atmospheric Sciences
in the Graduate College of the
University of Illinois at Urbana-Champaign, 2016

Urbana, Illinois

Advisers:

Assistant Professor Francina Dominguez

Abstract

The semi-arid Salt and Verde River basins in Arizona depend, in part, on Atmospheric River (AR)-related precipitation for meeting the water demands of the Phoenix metropolitan area. On the other hand, the region is also susceptible to AR-related flooding. In a warming climate, water vapor in the atmosphere increases, thus likely increasing the water vapor transport within ARs. To understand the precipitation-related impacts of climate change on extreme ARs affecting Arizona, a pseudo-global warming (PGW) method was used. High-resolution control and future simulations of five intense historical AR events that affected the Salt and Verde River basin in Central Arizona were carried out. Control simulations realistically captured the magnitude and spatial distribution of precipitation during all five events. The PGW approach for future simulations involved changing the initial and lateral boundary conditions of the input data. The climate change signals of several thermodynamic variables were obtained from an ensemble of 9 General Circulation Models for RCP 8.5 scenario. Two sets of perturbations were applied to the input data. The first set consisted of constant values of temperature change at different vertical levels (PGW1) and the second set consisted of spatially varying temperature values (PGW2). Future simulations showed an overall increase in integrated vertical transport of vapor and upward moisture flux at cloud base over the region for all events. The changes in precipitation at both domain and basin level were highly spatially heterogeneous. Precipitation at the basin level increased in all PGW1 simulations but showed a decrease for some PGW2 simulations. The domain-averaged precipitation increased in all future simulations but the increase remained sub-Clausius-Clapeyron for all but one PGW2 event in which shifting and significant strengthening of the low-level jet was observed. Melting levels rose by more than 600m in all future simulations and this led to a decrease in the fraction of frozen precipitation during the events by more than 80%.

ACKNOWLEDGMENTS

The author would like to thank his adviser Dr. Francina Dominguez for her valuable guidance and support. In addition, the author would like to thank Dr. Steve Nesbitt, Dr. Sonia Lasher-Trapp and Dr. Robert Trapp of the University of Illinois at Urbana-Champaign for their help. Support for this work was made possible by United States Geological Survey (USGS) Grant G15AP00082.

TABLE OF CONTENTS

CHAPTER 1

INTRODUCTION

Atmospheric Rivers (ARs) are long and narrow filaments of high Integrated Vapor Transport (IVT) that are responsible for about 90% of low-level meridional transport of water vapor in the atmosphere [*Zhu and Newell,* 1998]. They impinge upon the orography of the west coasts of continents to produce precipitation [*Neiman et al.,* 2008b]. ARs have been associated with several major flooding events along the west coasts of midlatitude North America and Europe [*Ralph et al.,* 2006; *Neiman et al.,* 2008a, 2011a; *Stohl et al.,* 2008; *Leung and Qian,* 2009; *Lavers et al.,* 2011]. In addition to causing precipitation over the mountain ranges along the West Coast of the United States, ARs can penetrate inland and cause precipitation and even flooding in states such Arizona [*Neiman et al.,* 2013; *Rivera et al.,* 2014; *Rutz et al.,* 2015].

ARs form a major component of winter precipitation over the southwestern US, particularly Arizona [*Knippertz and Martin,* 2007; *Dettinger,* 2011; *Rutz and Steenburgh,* 2012; *Neiman et al.,* 2013; *Rivera et al.,* 2014; *Rutz et al.,* 2014]. Arizona belongs to a water-deficient region of the country that is critically dependent on winter precipitation to fulfill the water demand of its population. Although Arizona receives up to 50% of its annual rainfall during the monsoon season from July through September [*Sheppard et al.,* 2002], the majority of this precipitation is lost due to high incoming solar radiation causing increased evapotranspiration rates. Winter precipitation also leads to snow accumulation in high elevation regions [*Bryson and Hare,* 1974; *Sheppard et al.,* 2002; *Neiman et al.,* 2013] which aids in replenishing reservoirs via snowmelt during the spring. *Dettinger et al.,* [2011] argued that the contribution of AR events to total cool season (November-April) precipitation in Arizona for water years 1998-2008 was less

than 10%, but they only included ARs that crossed the west coast of the US between 32.5^{o} N and 55^{o} N. However, *Rutz and Steenburgh* [2012] conducted a similar study but included ARs that crossed the west coast of Baja Peninsula (24^{o} N - 55^{o} N) as well. Their study showed that the percentage contribution of ARs to the cool season precipitation in AZ varies from about 10 % - 30 % with the value of contribution decreasing from western AZ to eastern AZ.

Along the lines of their previous study, *Rutz et al.,* [2014] determined the climatological characteristics of cool season (November–April) ARs and the resultant precipitation over the western US. Their results showed that the fraction of cool season AR-related precipitation in Arizona varies between 0.15 – 0.45 with values decreasing from southwestern AZ to northeastern AZ. They also showed that ARs affecting the southwestern US exhibit relatively lower frequency and higher duration. They concluded that a relatively small number of ARs are responsible for a large contribution to the total cool-season precipitation over the region making them critically important for the hydroclimate of this area. Additionally, they observed that ARs affecting the Southwest traverse the mountains of Southern California and the Baja Peninsula which are relatively narrow and discontinuous leading to reduced decay in AR frequency as the ARs penetrate inland. Rivera et al. [2014] discussed the climatological characterization of extreme inland penetrating ARs that affect the Verde River Basin in Central Arizona. Their study found that extreme ARs provided 10% - 50 % of the total cool season (November–March) precipitation in the region. Their analysis of SNOTEL data revealed that such ARs led to Snow Water Equivalent (SWE) increase of 25% - 35% of the seasonal peak SWE accumulation.

In addition to their contribution to mean winter precipitation in AZ, ARs can also cause intense precipitation leading to extreme flooding episodes. *Neiman et al.* [2013] provided a detailed synoptic, mesoscale and hydrometeorological analysis of extreme precipitation events

associated with a series of inland penetrating ARs that affected Central Arizona in January 2010. Their study also concluded that in order to reach Arizona, ARs must cross the mountainous range in Southern California and northern Baja.

ARs not only form an important part of the hydrological budget of the region but also deserve careful attention owing to the record-setting flooding events that they could cause. Hence, it is important to understand the changes in the ARs that could occur in a future climate. This holds especially true for extreme AR events due to their disproportionally high contribution to winter precipitation. There have been several studies that discuss possible future changes in the frequency and intensity of ARs affecting the western coasts of North America and the UK [*Dettinger*, 2011; *Lavers et al.*, 2013; *Gao et al.*, 2015; *Payne and Magnusdottir*, 2015; *Hagos et al.*, 2016]. These studies project an increase in the frequency and intensity of extreme ARs in future climate, posing an increased risk of AR-related flooding events. Most of these studies evaluate the changes in frequency and intensity of ARs by analyzing Global Climate Model (GCM) output. While this approach is helpful in providing a statistical overview of these changes, it omits the in-depth analysis of how individual storms could change because the coarse-resolution GCMs cannot capture the details of the storm dynamics and thermodynamics, particularly the interaction with regional topography. Also, literature on how future climate could change inland penetrating ARs, particularly those affecting the US Southwest is still limited.

Rivera and Dominguez [2016] analyzed results from several IPCC-AR4 GCMs and dynamically downscaled simulations from the North American Regional Climate Change Assessment Program [NARCCAP; *Mearns et al.*, 2009] to investigate the robustness of the projected variations in AR intensity and AR-related precipitation for the US Southwest. They found that AR-related precipitation in the region does not show an overall robust variation in the

future. In addition, they pointed out that some GCMs project a decrease in Relative Humidity (RH) over parts of the US Southwest which probably led to statistically robust reduction in the projected AR-related precipitation in the region. Keeping in mind the results of these studies, this study attempts to understand these changes in extreme AR-related precipitation events at the individual storm scale.

To achieve storm-scale understanding, one could either perform dynamical downscaling of select AR events as identified in the GCM output or follow a pseudo-global warming approach [*Schär et al.*, 1996b; *Sato et al.*, 2007; *Kawase et al.*, 2009; *Lynn et al.*, 2009; *Rasmussen et al.*, 2011; *Lackmann*, 2013, 2015]. The latter approach is particularly useful in addressing the question of how individual weather events that have happened in the past might change in a future climate owing to thermodynamical changes and will be used in the present study.

Pseudo-Global Warming (PGW), as introduced by *Schär et al.* [1996] involves adding projected large-scale thermodynamic perturbations to lateral and initial boundary conditions that are used to drive regional climate models. In their study, *Schär et al.* [1996] argued in favor of adding a constant perturbation temperature value to each pressure level while keeping RH and dynamics unchanged. However, many studies using the PGW approach do not add a constant perturbation value to the temperature field at different vertical levels. *Lackmann* [2013] conducted a study in which they used a PGW approach to examine the thermodynamical changes in pre-cold frontal Low Level Jet (LLJ) that led to a flooding event in south-central U.S. in May 2010. They perturbed temperatures at the 2-m level, sea surface, and pressure levels with spatially heterogeneous signals while keeping RH constant. They found that while LLJ did not strengthen in the future simulation, the precipitation increased significantly with 72-h total area

averaged value increasing by 43 %. They attributed this increase to the enhanced water vapor present in the future simulations.

It is argued that the projected increases in the intensity of extreme events, including ARs are mostly thermodynamic in nature [*Trenberth et al.*, 2003; *Emori*, 2005; *Lavers et al.*, 2013; *Payne and Magnusdottir*, 2015]. The primary reason for using the PGW approach in this study rather than dynamical downscaling of GCM data is that the PGW method allows us to isolate thermodynamically driven changes in the intensity of extreme events. *Hazeleger et al.*, [2015] argue that high-resolution simulations of extreme weather events from the past in a theoretical future climate have the potential to provide a meaningful and convincing picture of future weather and can aid in decision-making. Traditional dynamic downscaling (TDD) approach uses data from GCMs whose ability to predict future climate is compromised by model inadequacies and uncertainties [*Stainforth et al.*, 2007]. Additionally, PGW approach can be relatively computationally efficient.

In this study, we evaluated how extreme ARs affecting the Salt and Verde River Basins (SVRB) in AZ could change in the future owing to thermodynamical changes while keeping RH constant. That is, if the synoptic pattern associated with these extreme ARs were to be replicated in a future climate towards the end of the twenty-first century, how would the intensity and spatial distribution of the resultant precipitation in the region change due to thermodynamic changes only.

Five intense atmospheric river events representing a variety of synoptic conditions were dynamically downscaled using the Weather Research and Forecast (WRF) model [*Skamarock et al.*, 2008]. Subsequently, the driving fields were perturbed to run PGW simulations. Two sets of

PGW simulations were carried out with two different sets of perturbation values. The next section describes the data and methods employed in the study. Section 3 describes the main findings of the study. It compares the control simulations with observations and evaluates how the future simulations differ from the control simulations. It also presents a brief synoptic analysis of two of the five events. Section 4 summarizes these findings.

CHAPTER 2

DATA AND METHODOLOGY

2.1 Selection of events and model setup

Five major AR events that affected the SVRB were selected based on the top annual daily cool season (November – March) streamflow values in the Salt River (USGS site no.: 09497500) for the period 1980-2015. These peak streamflow dates were compared against a list of ARs that affected SVRB. These ARs were identified in Modern Era Retrospective-Analysis for Research and Applications (MERRA) data [*Rienecker et al.*, 2011] using an algorithm proposed by *Lavers et al.* [2012]. The algorithm uses an IVT threshold to iteratively locate points of interest in order to identify intense ARs that penetrated into SVRB. The peak streamflow dates that coincided with AR events in the region were selected and arranged in decreasing order of intensity. Table 1 shows the details of five most intense AR-related streamflow events.

The WRF model was used to simulate each of the five AR events. ERA-Interim reanalysis [*Dee et al.*, 2011] data was used for initial and lateral boundary conditions in the Control simulations. The domain setup included three domains with horizontal resolutions of 27 km, 9 km and 3 km (Figure 1a) with 40 vertical levels. Since most of the AR-related precipitation in the region is orographic in nature [*Neiman et al.*, 2013], a high resolution inner domain was required [*Hughes et al.*, 2014] to appropriately simulate the interaction of ARs with regional topography. Figure 1b shows the extent of the innermost domain and the regional topography. It also shows location of the two basins of interest- Salt River Basin (SRB) and Verde River Basin (VRB). Some preliminary simulations with the innermost domain excluding the mountains in Southern California and the Baja range were also conducted. However, these

simulations severely underestimated precipitation (not shown) in the basin with the 2008 simulation producing almost negligible precipitation. This highlights the importance of correct representation of the topography in modeling these events. Temperature, geopotential and winds fields corresponding to the outermost domain were continuously nudged [*Miguez-Macho et al.*, 2004] to the input fields every 6 hours. This was done to retain the large scale features of atmospheric circulation during the simulations. Through some initial sensitivity tests, it was found that spectral nudging specifications were critical in correctly simulating AR-related precipitation. The model setup included Morrison 2-moment microphysics scheme [*Morrison et al.*, 2009], RRTMG shortwave and longwave radiation schemes [*Iacono et al.*, 2008], the Noah Land Surface Model [*Tewari et al.*, 2004], Yonsei University boundary layer scheme [*Hong et al.*, 2006] and Kain-Fritsch cumulus parameterization [*Kain*, 2004]. The above mentioned model setup was used for both control and PGW simulations. For evaluating the model performance, the model precipitation output was compared with a gridded daily average precipitation dataset with a resolution 1/16 of a degree [*Livneh et al.*, 2013; hereafter referred to as Livneh dataset].

2.2. Calculation of perturbations

Two sets of perturbations were used in the PGW method. To compute these perturbations, gridded datasets containing mean monthly values of air temperature (T) at different pressure levels, near surface air temperature (Ts), sea-surface temperature (SST) and soil temperature (ST) for the months of December, January and February (DJF) were used. In all, data from 9 GCMs for the past (historical experiment) and future (RCP8.5 scenario) periods was obtained from the CMIP5 archive (https://pcmdi.llnl.gov/projects/esgf-llnl/). Table 2 provides a brief description of these models. The RCP scenarios represent different values of Greenhouse Gas (GHG)-caused radiative forcing by the year 2100 [*van Vuuren et al.*, 2011]. Subsequently,

the GCM data was regridded to the horizontal resolution and vertically interpolated to the set of pressure levels corresponding to ERA-Interim data. Multi-model ensembles of the above-mentioned variables for historical (1980-2004) and far future (2071-2098) periods were calculated, and averaged over the DJF season. *Lauer et al.*, [2013] conducted several PGW downscaling experiments over Hawaii using climate change signals from 10 CMIP5 models for RCP4.5 and RCP8.5. They found that while the results varied significantly between different models, the results obtained using multi-model mean are very similar to the ensemble mean of experiments using signals from individual models.

Finally, the projected changes (hereafter, deltas) in the winter time values of these variables were obtained by subtracting the historical mean DJF fields from the respective future fields. Here, the first set of deltas was obtained by averaging the projected changes in surface variables and 3-D variables at different pressure levels over the area of the outermost domain. We denote the set of simulations using these horizontally-homogeneous deltas as PGW1. Figure 2 shows the vertical profile of delta air temperature. The second set of deltas is the spatially varying projected changes obtained by the procedure described in the preceding paragraph. Figure 3 shows delta values of air temperature at 850mb, 500mb and 300 mb pressure levels and delta values of Ts and SST over the largest domain. The higher changes in land surface temperature when compared to the sea surface temperature are seen in Figure 3d. We denote the second set of simulations using horizontally-heterogeneous deltas as PGW2.

The two sets of delta values not only provide different initial and boundary conditions for the simulations but also represent plausible future climate scenarios. In the first set of simulations, constant delta values at different levels can provide first-order thermodynamic only changes in extreme AR-related precipitation as the dynamics of the storms do not change [*Schär*

et al., 1996a]. The second set of spatially heterogeneous deltas could help incorporate regional temperature gradients projected by these models into the simulations and therefore provides for another reasonable future climate setting to estimate the changes in these events. Comparing the two sets of experiments also highlights the sensitivity of the storms to, relatively minor, horizontal gradients in temperature.

Both sets of deltas were then added to the input ERA reanalysis used in the control simulation. After the perturbation of input data with the computed climate change signals, the five events were simulated again twice (PGW1 and PGW2) using WRF and with identical domain setup, time period and physics as the Control simulations.

CHAPTER 3

RESULTS

3.1 Control Simulations

The precipitation output from Control simulations was compared with precipitation from Livneh dataset. Figure 4 shows the daily average precipitation (mm/d) during the entire duration of the 5 events from Livneh dataset and WRF Control simulations. It should be noted that during the Jan 2010 event, 3 ARs affected the region from 19 Jan to 22 Jan with the third AR being the most intense [*Neiman et al.*, 2013]. Thus, the precipitation in Figures (i)-(j) represent the average precipitation due to 3 individual ARs over the course of 4 days. Similarly, for the 1991 event, two ARs affected the region from 28 Feb to 2 Mar 1991. For the events in 1980, 1993 and 2008, only one AR affected the SVRB during the time interval of the simulation. In reality, several ARs affected SVRB during the Jan-Feb 1993 but for the purpose of this study, the first AR, which also happened to lead to the largest annual streamflow value in the Salt River, was chosen. The averaging period for each event in Figure 4 depends on the duration of the AR-caused precipitation and is mentioned in the caption of the figure.

The purpose of this comparison is to determine how the model simulates the intensity and spatial distribution of AR-related precipitation in SVRB. In the case of the Feb 1980 event, the model was able to capture the spatial distribution of the precipitation in the northern SRB. However, it overestimated precipitation at the eastern edge of the SRB. In the Feb-Mar 1991 event, the model overestimated precipitation in SRB but underestimated in VRB. In the Jan 1993 event, the model reproduced the outer extent and spatial pattern of the precipitation to a large degree; however, it underestimated the overall precipitation in the SVRB. In case of Jan 2008 event, the model performed well in constraining most of the precipitation to the SRB but it was

not able to resolve finer details of precipitation distribution. For the Jan 2010 event, the model did well in reproducing the precipitation pattern in central SRB but could not reproduce precipitation well in other parts of the basin. It can also be observed from Figure 4 that the various AR events affect different parts of the region to different degrees. For example, the January 2008 event resulted in higher precipitation in the SRB than the VRB. This occurs because AR-related precipitation depends critically on the angles of impingement upon the topography [*Neiman et al.*, 2011b]. Figure 5 shows the comparison between daily basin-averaged precipitation from Livneh dataset and WRF output. WRF is able to capture the temporal distribution of precipitation in the region. Figure 5 also shows that WRF tends to underestimate the basin-averaged precipitation. However, towards the end of the event, it generally overestimates precipitation. Thus, while there are some small spatial and temporal differences, the control simulations were able to realistically capture the overall magnitude, spatial and temporal variation of the precipitation during these five events given the complex terrain in the region. This instills confidence in the model setup.

3.2 PGW simulations

In the PGW simulations, the average temperature increase in the lower troposphere is more than 4 K. According to the Clausius-Clapeyron (C-C) relation, if RH remains constant, the saturation vapor pressure must increase by about 30 % (~ 7% increase per K rise in temperature). If storm dynamics is remains unchanged with respect to the Control simulations, one must expect about 30% increase in IVT and a similar change in upward moisture fluxes assuming that atmospheric stability does not change significantly.

Analysis of model output shows that synoptic-scale conditions in all future simulations are very similar to those in the control simulations. Figures 6 and 7 show the changes in daily mean precipitation during the five events for PGW1 and PGW2 simulations, respectively. It can be seen that the changes in precipitation in the future simulations are highly spatially heterogeneous. Tables 3 and 4 show the fractional changes in basin- and domain (innermost)-averaged event-accumulated precipitation for all five events for PGW1 and PGW2 simulations, respectively. The event-averaged precipitation over the basin increases in all the PGW1 runs, with fractional changes varying from 3.6% for the 2008 event to 36% for the 1993 event. The fractional changes in domain-averaged precipitation vary from about 11% for the 1993 event to 22.6% for the 1991 event. Thus, overall increase in precipitation at the domain-level is sub-C-C in all the cases. Except for the 1993 PGW1 run, the precipitation changes at basin level are also sub-C-C.

IVT shows an overall increase in both sets of simulations (Figure 8). For the purpose of this study, we define large-scale precipitation efficiency of an AR event over an area as the ratio of the total upward moisture flux at the base of the cloud (or the Lifting Condensation Level (LCL)) to the total precipitation flux averaged over the area and over duration of the event. Figure 9 shows the time series of these fluxes for different events for all sets of simulations. Precipitation efficiency for a given simulation can then be calculated as the ratio of areas under the precipitation and moisture flux curves. It can be observed that upward moisture fluxes increase in the PGW simulations with the fluxes in PGW1 and PGW2 simulations following a similar pattern. For the PGW1 simulations, the relative increase in upward moisture flux at LCL varies from 32.8% for the 1980 event to 44.6% for the 2008 event (Table 3). The changes in domain-wide Precipitable Water (PW) closely follow the C-C relation (~31%). Clearly, the

changes in upward moisture flux and PW do not translate linearly into changes in precipitation. These results indicate that the precipitation efficiency in all five PGW1 events decreases when compared to the Control simulations.

Similar to the PGW1 simulations, the changes in precipitation in the PGW2 simulations span a much larger range than the changes in moisture flux. The relative changes in domain-averaged precipitation for PGW2 are all positive with values varying from 1.3 % for 1993 event to about 57 % for the 2008 event (Table 4). Barring the 2008 event, the precipitation changes at the domain-level are sub-C-C in this set of simulations as well. As far as changes in event-averaged basin-averaged precipitation are concerned, there is no clear pattern. The relative changes in the basin-averaged control precipitation during the events vary from about -9% for the 1991 event to about 23 % for the 2008 event. The fractional increase in upward moisture flux at LCL varies from 25.8% for the 1980 event to 54.1% for the 2008 event. For PGW2 simulations, domain-averaged PW increases in accordance with the C-C equation for all events except the 2008 event The precipitation efficiency remains about the same for the 1980 PGW2 event and decreases for all but the 2008 event.

In the PGW2 simulations, the addition of spatially heterogeneous temperature perturbations implies that the dynamics can change when compared to the Control simulation (see *Schär et al.*, [1996a] for a mathematical derivation). Still, the large-scale dynamics of the events remains very similar to the control simulations. While the IVT tends to increase in the future for all the PGW2 events (Figure 8), changes in the strength of LLJ are different for different events and at different times during the simulation (Figure 10). For example, the 2008 PGW2 event shows a slight shift and significant increase in the strength of LLJ causing a super-C-C increase in precipitation.

In addition to precipitation, changes in melting level are also analyzed. Table 4 shows the absolute and fractional changes in event-averaged basin and domain-averaged melting level (ML) for all the PGW simulations and the five events. Melting level is raised in all the PGW simulations at both the basin and domain level. Consequently, the ratio of frozen to total precipitation (FR) decreases. For the PGW1 simulations, the domain-averaged relative changes in FR vary from -85% for the 1991 event to -94 % for the 1980 and 1993 events. The basin-averaged changes in FR for PGW1 simulations show similar magnitude. PGW2 simulations also show similar changes in FR over the basin and domain.

CHAPTER 4

SUMMARY AND CONCLUSIONS

Several studies have indicated that extreme AR events are likely to become stronger in the future, primarily due to thermodynamic changes [*Lavers et al.*, 2013; *Gao et al.*, 2015; *Payne and Magnusdottir*, 2015]. This could lead to severe flooding events and therefore could threaten human populations and ecosystems. In particular for the semiarid Southwestern United States, changes in the intensity of extreme ARs could have significant impacts on the region's water resources and infrastructure. In the case of Arizona, extreme ARs form an important part of cool season precipitation over the region and have led to severe flooding events in the past [*Neiman et al.*, 2013; *Rivera et al.*, 2013; *Rutz et al.*, 2015]. In this study, we evaluated how five extreme AR events that affected the Salt and Verde River basins in Arizona could potentially change in a future climate. *Hazeleger et al.*, [2015] argue that the information obtained by simulating past extreme weather events in different future climate settings could prove more useful and relevant to decision-makers and stakeholders than results from traditional downscaling of Climate Model data. These simulations can be used to analyze event types selected by users and could use various plausible boundary conditions representative of future climate. This could help provide important information to aid in the design of infrastructure whose strength is tested by the most extreme events. Pseudo-Global Warming approach forms part of this larger methodology proposed by *Hazeleger et al.*, [2015]

A Pseudo-Global Warming approach was used to simulate how extreme landfalling future ARs in the region would respond to thermodynamical changes. We did this by perturbing the historical conditions with projected temperature changes obtained from an ensemble of

GCMs and then simulating the events using high-resolution WRF model. Two sets of perturbations were applied – the first set consists of homogeneous changes in temperature values at a given level (PGW1) and the second set consists of spatially heterogeneous temperature change values (PGW2). Relative humidity was kept constant in all cases by modifying specific humidity.

Analysis of the Control simulations revealed that the model was able to capture the general magnitude and spatial pattern of precipitation in the basin for all five selected events. We found that the extent of the domain and specifics of spectral nudging parameters were critical in realistically representing precipitation. Overall, domain-averaged precipitation increased in all the PGW simulations. For the PGW1 simulations, basin-averaged precipitation increased in PGW1 simulations (3.6% for the 2008 event to 36% for the 1993) demonstrating the likelihood of increased precipitation in the basin in future owing solely to thermodynamic changes. The relative changes in domain-averaged precipitation vary from about 11% in the 1993 event to 22.6% for the 1991 event. The relative increase in upward moisture flux at LCL varies from 32.8% for the 1980 event to 44.6% for the 2008 event, for the PGW1 simulations. Precipitation efficiency decreases for all events in PGW1 simulations. For PGW2 simulations, the fractional changes in domain-averaged precipitation vary from 1.3 % for 1993 event to about 57 % for the 2008 event. Fractional changes in the precipitation over the basin during the event vary from about -9% for the 1991 event to about 23 % for the 2008 event. In the PGW2 simulations, the fractional increase in upward moisture flux at LCL varies from 25.8% for the 1980 event to 54.1% for the 2008 event. Except for the 2008 event, precipitation efficiency remains the same or decreases in PGW2 simulations. *Trenberth*, [1999] argue that in a warmer climate, depending upon the relative humidity, more moisture might remain in the atmosphere after precipitation.

So, the increase in precipitation may be lesser than the increase in moisture indicating that the precipitation efficiency decreases.

Several studies examine the scaling of a variety of extreme precipitation events with the C-C relation [*Pall et al.*, 2007; *Lenderink and van Meijgaard*, 2008; *Wasko et al.*, 2015]. The exact physical processes that govern the changes in extreme precipitation with changing atmospheric temperatures should depend upon the location, dynamics and thermodynamical conditions of the event [*Diffenbaugh et al.*, 2005; *Wasko et al.*, 2015]. Since PGW2 simulations included some dynamical changes to LLJ in addition to the thermodynamic changes, the large variation in basin-averaged precipitation in PGW2 simulations shows that basin precipitation is very sensitive to changes in the jet orientation and strength. The changes in precipitation for all the five events in both sets of future simulations are highly spatially heterogeneous due to the complex nature of the terrain. Overall, the domain-averaged precipitation showed a sub-Clausius-Clapeyron rate of change in most of the PGW simulations. This is similar to the results obtained by *Siler and Roe*, [2014] who also found that the total precipitation in their idealized simulation of a strong orographic AR-like event increased by a fraction smaller than near-surface water vapor.

The changes in domain-averaged precipitation showed a much larger variation than the upward moisture fluxes, highlighting the complex multi-scale nature of precipitation. The 2008 PGW2 event exhibited a slight shift and strengthening of the jet which led to an increase of about 57% in the domain-averaged precipitation. This strengthening may be the result of dynamical feedback induced by increased condensational heating in the future climate [*Lackmann*, 2002, 2013]. *Shi and Durran*, [2016] argue that the sensitivity of extreme orographic precipitation to warming is lower than that over the oceans and plains. However, in case of ARs affecting AZ

and other regions, while the precipitation is mostly orographic in nature, other factors such as the orientation and strength of the jet (particularly, at basin level) and low level moisture convergence [*Dacre et al.*, 2014] are also very important. Hence, sensitivity of cyclone dynamics over oceans to rising temperatures should also play important role in governing the overall sensitivity of basin-level AR-related extreme precipitation to climate warming.

The melting level values over the basin during the future events were raised by more than 800m in certain cases. Analysis of PGW simulations revealed that the fraction of precipitation falling as liquid form (as opposed to solid form) increased considerably in the future simulations. Increased fraction of liquid precipitation in future simulations could lead to the increased possibility of 'rain-on-snow' events in the future climate and therefore has the potential to amplify AR-related flooding in the basin [*Leung et al.*, 2004]. This could also lead to reduction in snow accumulation at high elevation and a subsequent decrease in snowmelt during the spring [*Mote*, 2003]. It could also affect winter tourism in several Indian reservations in the region. The value of accumulated precipitation over the domain and the basin increased in many PGW simulations while the duration of the events remained the same as control simulations. Thus, overall rain rate increased in many simulations. But more importantly, there are regions within the basins that received more than 50 mm d^{-1} of precipitation during the past events and experienced an increase of more than 25 mm d^{-1} (e.g. parts of VRB for 1980 PGW1) in some future simulations, thereby increasing the likelihood of severe local flooding in future climate.

Finally, it must be noted that while the PGW approach cannot predict changes in the frequency of ARs affecting the region, it can provide meaningful insights into how future extreme ARs could affect the region. The number of PGW simulations of extreme AR events can be extended to include other likely future climate scenarios and settings. The results obtained by

this study can be used as an input to hydrologic models in order to simulate streamflow and other variables that could be of interest to the water managers and decision-makers. Even in hydrologic simulations, several scenarios with varying antecedent soil moisture (and/or other variables) can be employed to test the hydrologic responses of the basin under different conditions and thus aid in preparedness and planning for extreme events.

TABLES

Table 1 Top 5 streamflow events in the Salt River coinciding with AR events

Event #	Peak streamflow date	Peak streamflow value (cfs)	WRF simulation period
1	15 February 1980	58,300	08-02-1980 00:00 – 17-02-1980 00:00
2	2 March 1991	38,800	21-02-1991 00:00 – 04-03-1991 00:00
3	8 January 1993	76,600	01-01-1993 00:00 – 12-01-1993 00:00
4	28 January 2008	55,300	22-01-2008 00:00 – 04-02-2008 00:00
5	22 January 2010	37,000	13-01-2010 00:00 – 24-01-2010 00:00

Table 2 Description of CMIP5 models used in the study

Model	Institution	Atmospheric Resolution (lon x lat)	No. of vertical levels	Reference
BCC-CSM1.1	Beijing Climate Center, China Meteorological Administration, China	2.8 X 2.8	26	Xiao-Ge et al. [2013]
CCSM4	National Center for Atmospheric Research, United States	1.24 X 0.94	26	Gent et al. [2011]
IPSL-CM5A-LR	Institut Pierre-Simon Laplace, France	3.75 X 1.8	39	Dufresne et al. [2013]
MIROC5	Atmosphere and Ocean Research Institute (The University of Tokyo), National Institute for Environmental Studies, and Japan Agency for Marine-Earth Science and Technology	1.4 X 1.4	40	Watanabe et al. [2010]
MIROC-ESM	Japan Agency for Marine-Earth Science and Technology, Atmosphere and Ocean Research Institute (The University of Tokyo), and National Institute for Environmental Studies	2.8 X 2.8	80	Watanabe et al. 2010
NorESM1-M	Norwegian Climate Centre, Norway	2.5 X 1.9	26	Zhang et al. [2012]
GFDL-CM3	Geophysical Fluid Dynamics Laboratory, United States	2.5 X 2	48	Donner et al. [2011]
GFDL-ESM2M	Geophysical Fluid Dynamics Laboratory, United States	2.5 X 2	48	Donner et al. [2011]
HadGEM2-ES	Met Office Hadley Centre , United Kingdom	1.875 X 1.25	60	Jones et al. [2011]

Table 3 Fractional changes (%) in different variables in PGW1 simulations with respect to Control simulations

Event Duration	Basin-Averaged Precipitation	Domain-Averaged Precipitation	Domain-Averaged Upward Moisture Flux at LCL	Precipitation Efficiency for Control Runs (%)	Precipitation Efficiency for PGW1 Runs (%)	Domain-Averaged PW
14 -15 Feb 1980	4.8	20.8	32.8	9.46	8.56	30.61
28 Feb - 2 Mar 1991	4.2	22.6	37.9	11.78	10.52	32.21
6 - 8 Jan 1993	36.0	10.9	37.1	13.35	10.58	30.00
27 - 28 Jan 2008	3.6	12.0	44.6	12.90	10.12	31.61
20 -22 Jan 2010	10.0	13.3	37.1	11.81	9.73	31.71

Table 4 Same as Table 3 but for PGW2

Event Duration	Basin-Averaged Precipitation	Domain-Averaged Precipitation	Domain-Averaged Upward Moisture Flux at LCL	Precipitation Efficiency for Control Runs (%)	Precipitation Efficiency for PGW2 Runs (%)	Domain-Averaged PW
14 -15 Feb 1980	- 4.2	24.2	25.8	9.46	9.46	32.80
28 Feb - 2 Mar 1991	-8.5	21.6	32.0	11.78	10.82	33.71
6 - 8 Jan 1993	19.2	1.3	27.9	13.35	10.29	33.09
27 - 28 Jan 2008	22.8	56.9	54.1	12.90	13.51	40.63
20 -22 Jan 2010	-3.7	13.3	9	11.81	9.20	34.00

Table 5 Fractional changes (%) in domain and basin averaged ML and FR for PGW1 and PGW2 simulations for the five events. The values in brackets are the absolute changes in ML in meters.

Event Duration	Basin-Averaged ML PGW1	Domain-Averaged ML PGW1	Basin-Averaged ML PGW2	Domain-Averaged ML PGW2	Basin-Averaged FR PGW1	Domain-Averaged FR PGW1	Basin-Averaged FR PGW2	Domain-Averaged FR PGW2
14 -15 Feb 1980	25.9 (690)	24.3 (727)	28.0 (750)	26.9 (807)	-89	-94	-90	-92
28 Feb - 2 Mar 1991	28.7 (661)	28.7 (823)	27.4 (633)	29.8 (856)	-82	-85	-84	-87
6 - 8 Jan 1993	30.1 (789)	26.9 (823)	31.9 (836)	28.8 (884)	-91	-94	-93	-95
27 - 28 Jan 2008	26.2 (696)	25.7 (771)	28.9 (766)	27.7 (833)	-95	-93	-95	-95
20 -22 Jan 2010	28.8 (636)	29.3 (791)	30.2 (668)	31.2 (841)	-79	-80	-80	-81

FIGURES

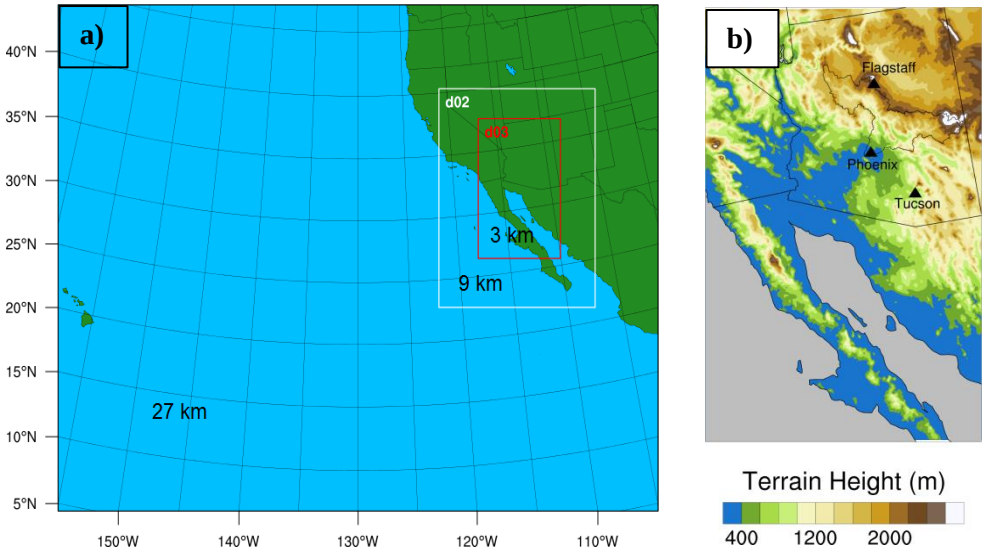

Figure 1 (a) WRF domain configuration (b) Terrain map of the innermost domain

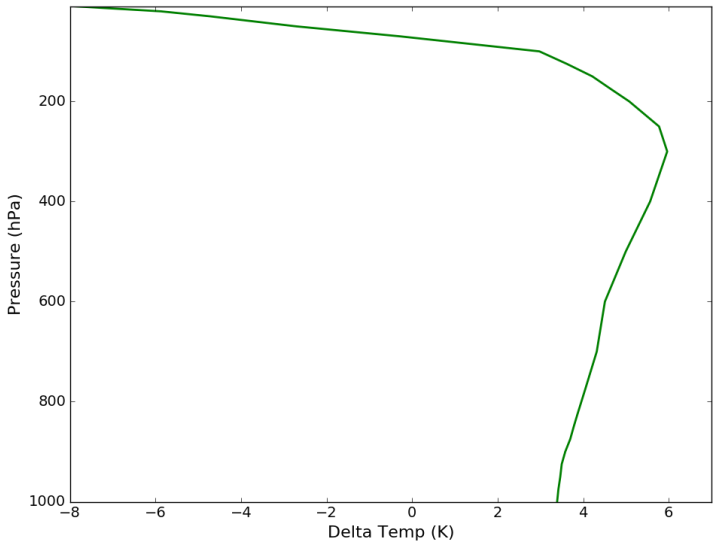

Figure 2 Vertical Profile of homogenous delta Temperature

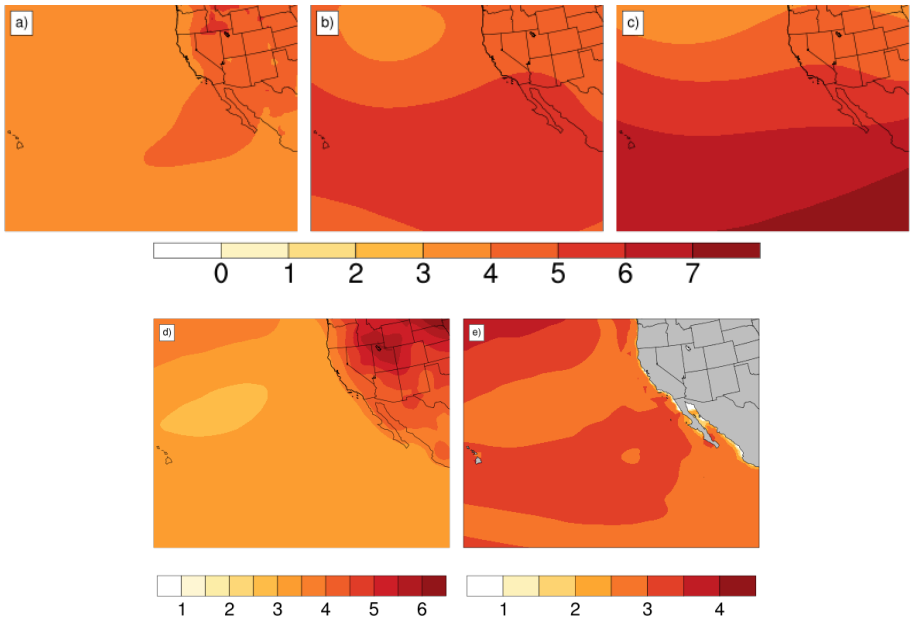

Figure 3 Delta air temperature (K) values at (a) 850 mb (b) 500 mb (c) 300 mb; (d) Delta near-surface air temperature (K) values (e) Delta SST (K). All deltas are for RCP8.5 scenario

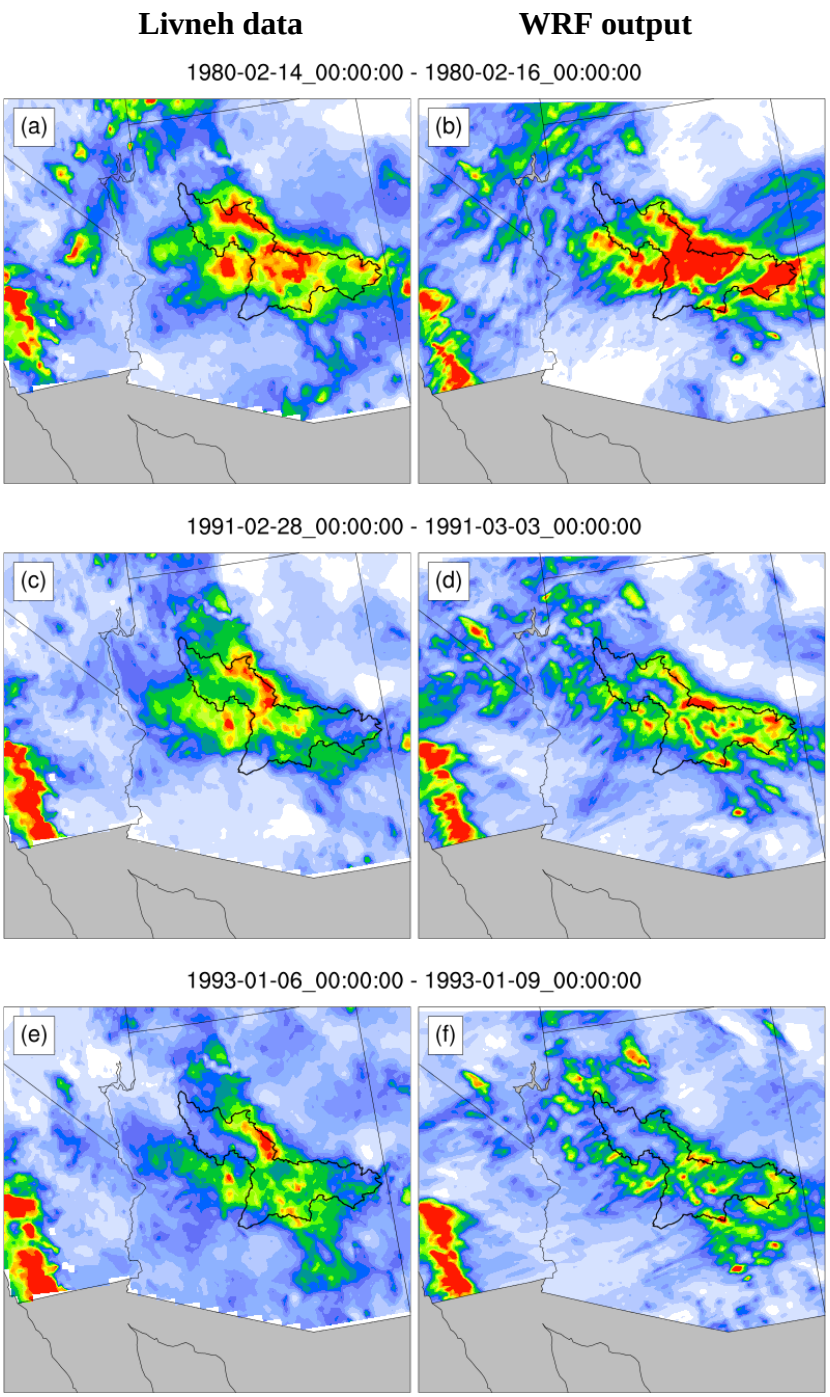

Figure 4 Comparison between Livneh data (left) and WRF precipitation output (right): (a)-(b) Daily average precipitation (mm/d) from 14-15 Feb 1980, (c)-(d) Same as in (a)-(b) but from 28 Feb – 2 Mar 1991, (e)-(f) Same as in (a)-(b) but from 6-8 Jan 1993, (g)-(h) Same as in (a) but from 26-28 January 2008 , (i)-(j) Same as in (a)-(b) but from 19-22 Jan 2010

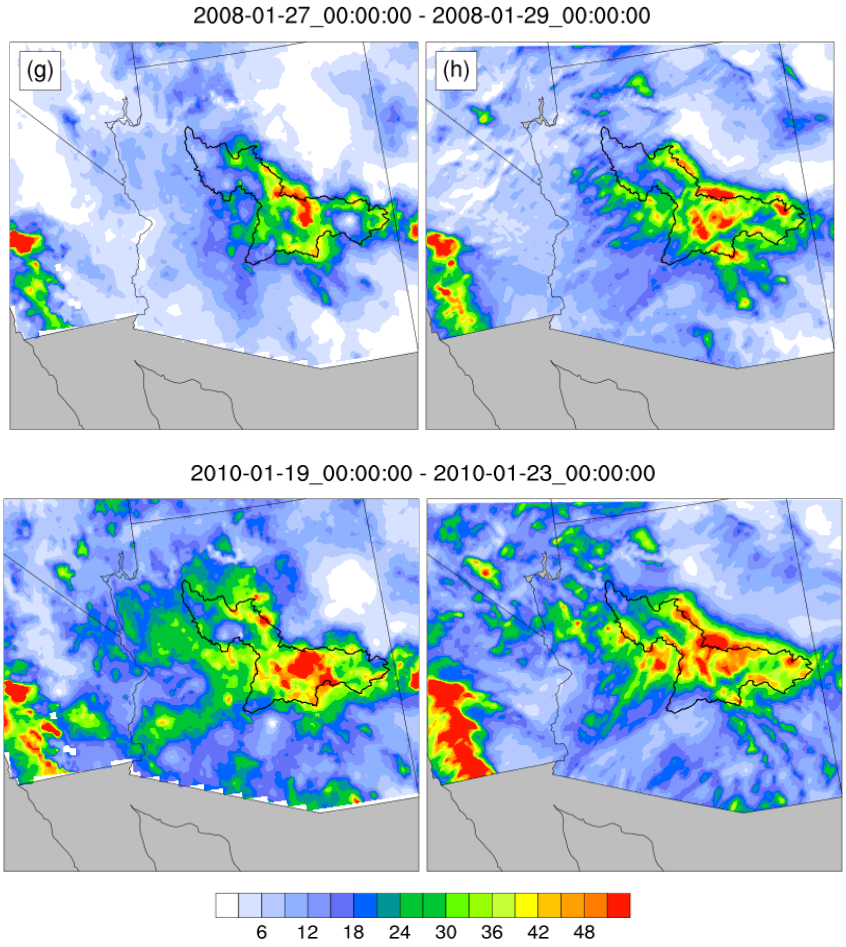

Figure 4 (cont.)

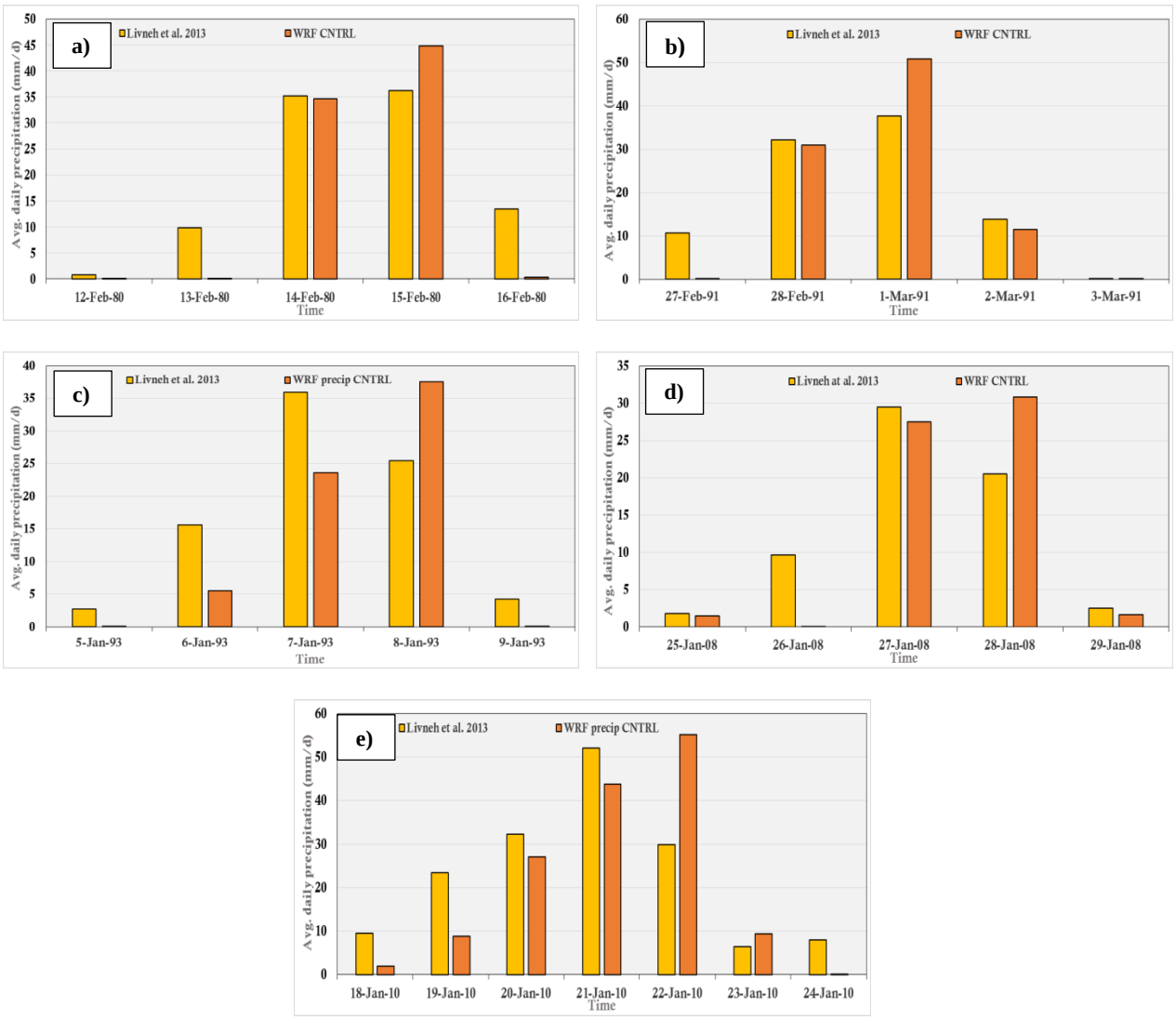

Figure 5 Comparison between daily basin averaged precipitation (mm/d) from Livneh dataset and WRF Control simulation output for the event in (a) 1980, (b) 1993, (c) 1991, (d) 2008, (e) 2010

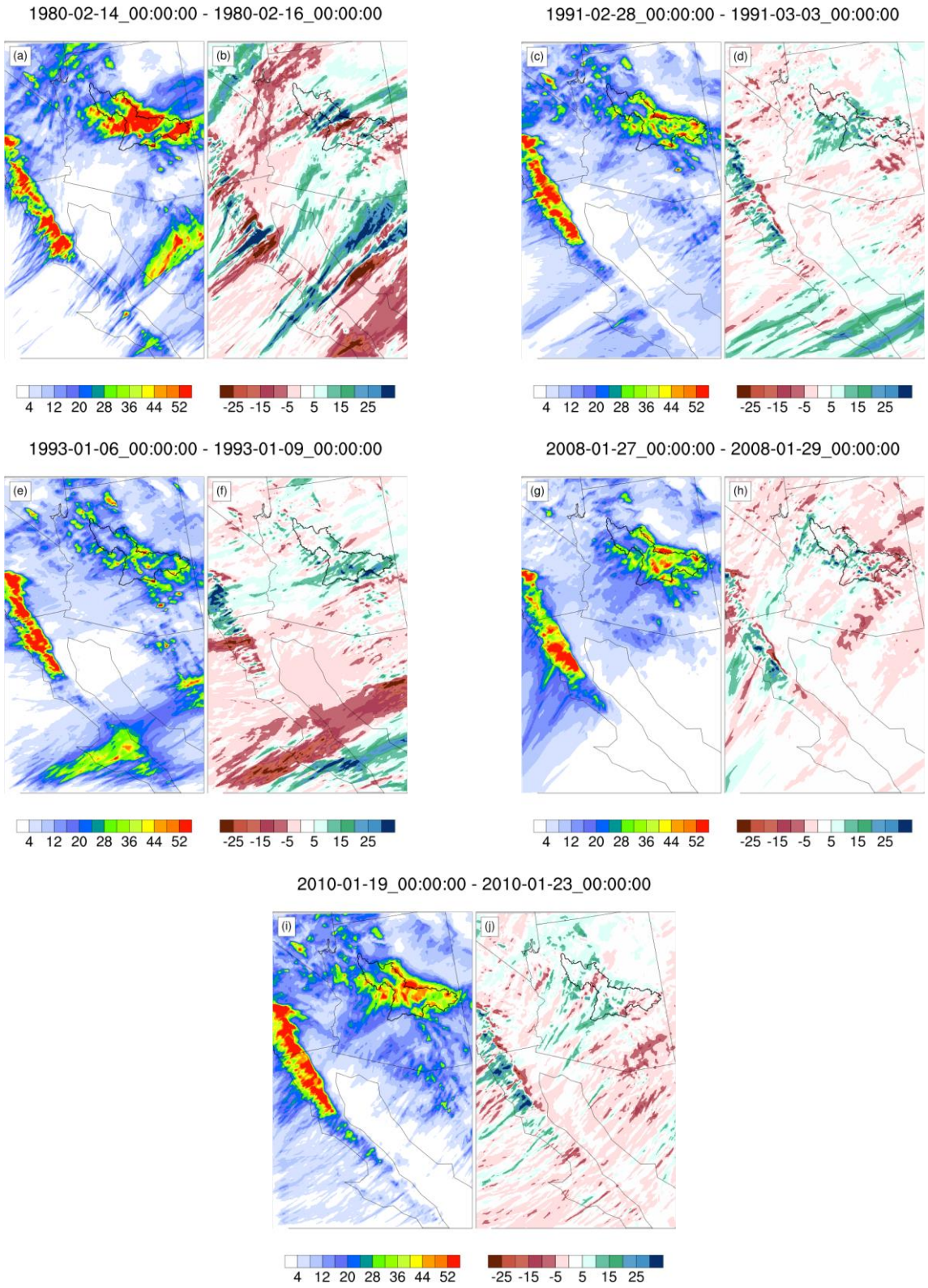

Figure 6 WRF Control precipitation output (left) and difference between Control and PGW1 simulations precipitation (right): (a)-(b) Daily average precipitation (mm/d) from 14-15 Feb 1980, (c)-(d) Same as in (a)-(b) but from 28 Feb – 2 Mar 1991, (e)-(f) Same as in (a)-(b) but from 6-8 Jan 1993, (g)-(h) Same as in (a) but from 26-28 January 2008 , (i)-(j) Same as in (a)-(b) but from 19-22 Jan 2010

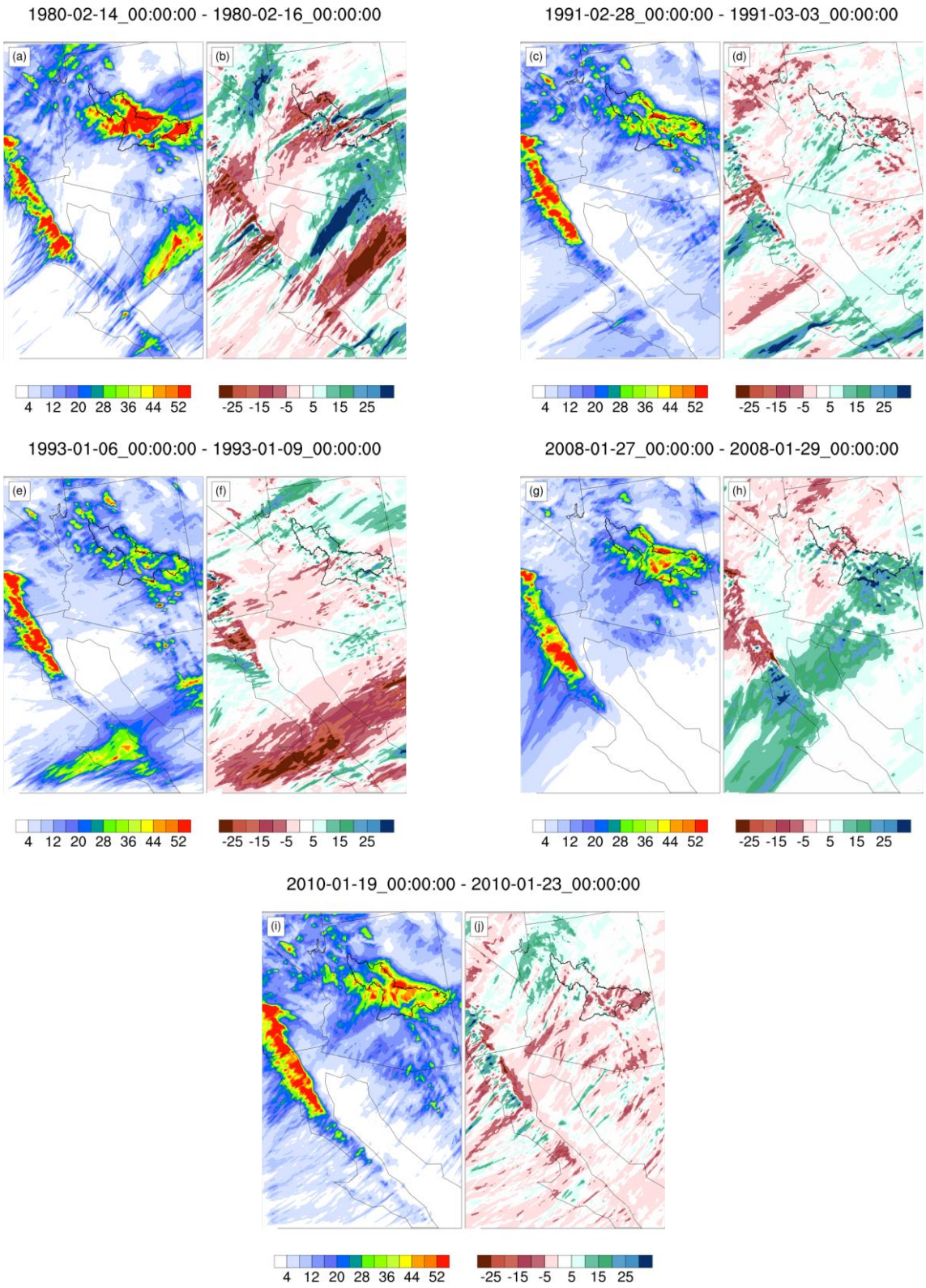

Figure 7 Same as Figure 8 but for PGW2 simulations

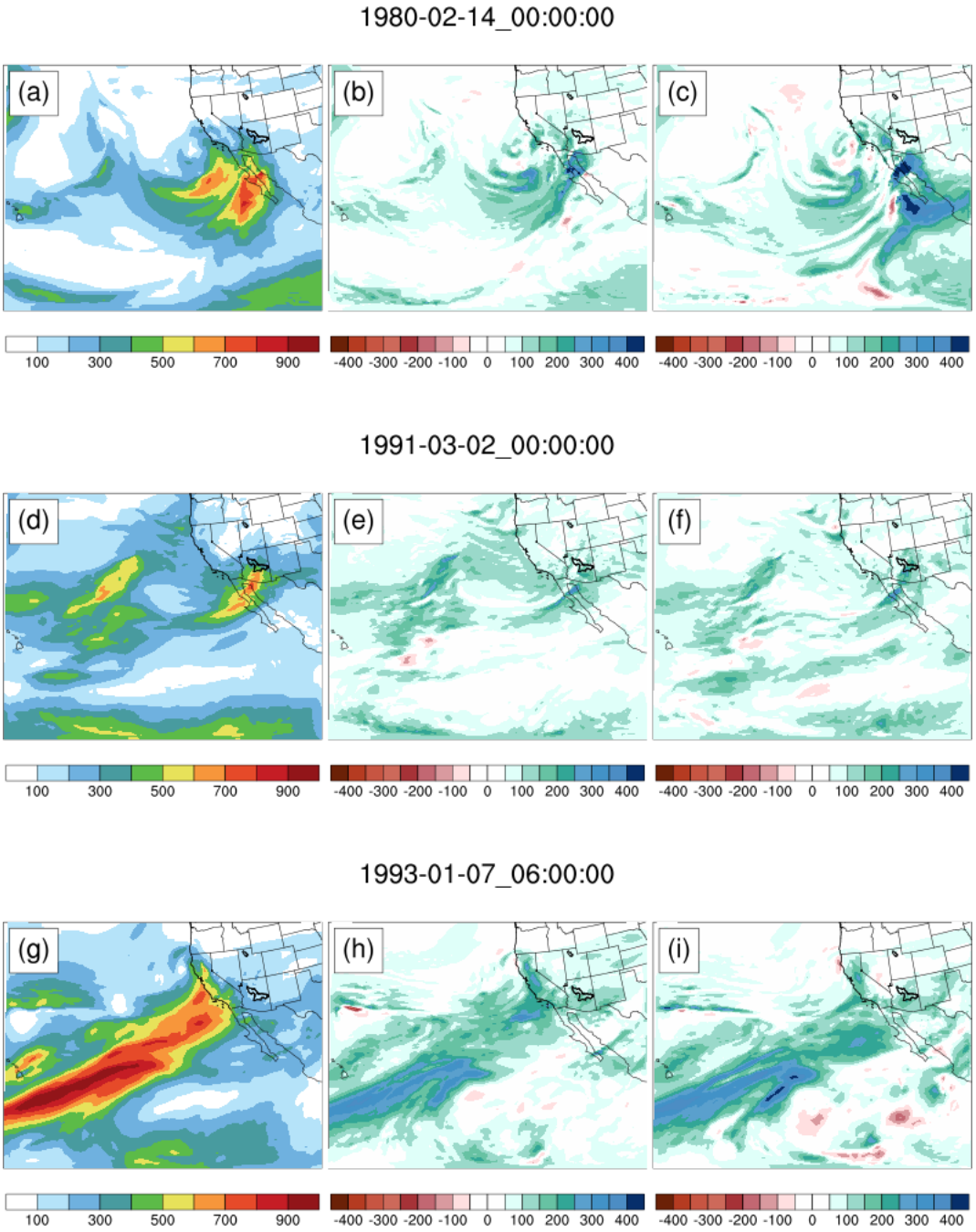

Figure 8 IVT (kg/m/s) for Control simulations (left column), difference between PGW1 and Control IVT field (middle column) and, difference between PGW2 and Control IVT field (rightmost column) for different events at specific times during the simulation. The time is indicated above each plot.

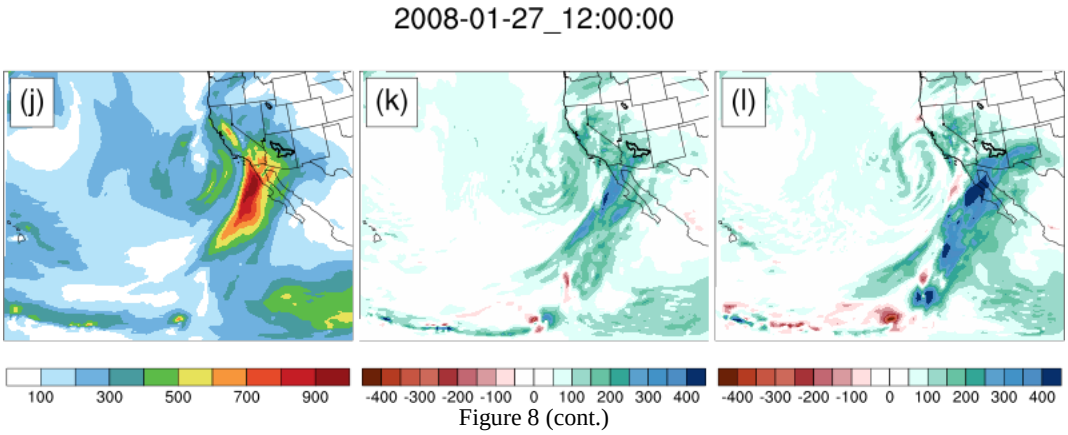

Figure 8 (cont.)

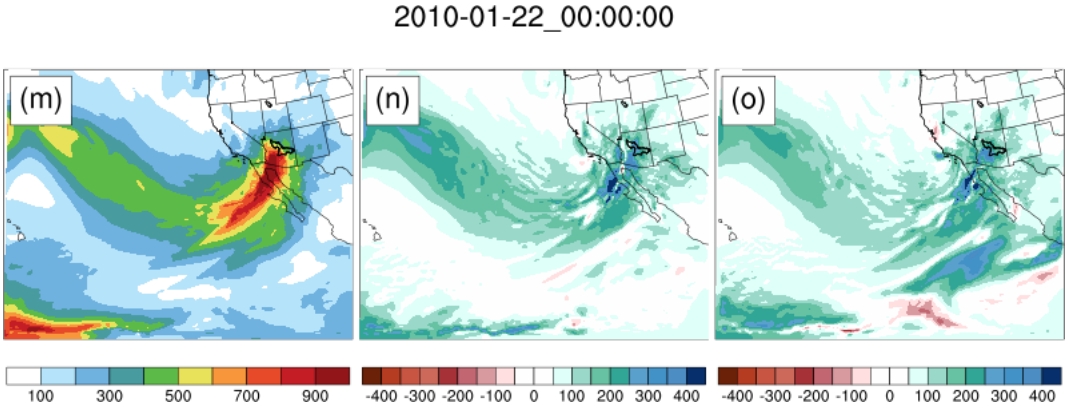

Figure 8 (cont.)

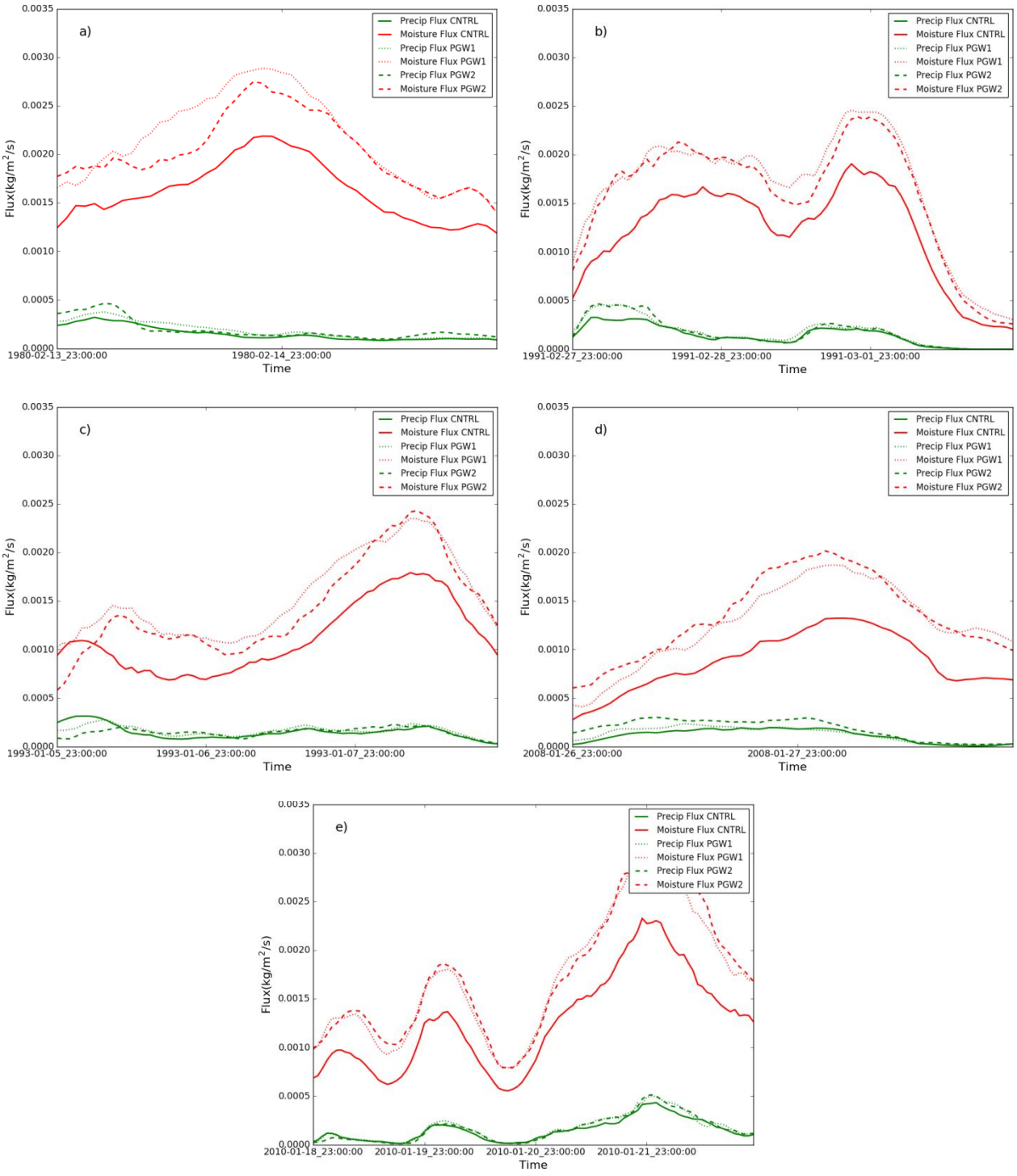

Figure 9 Time series of upward moisture flux at LCL and precipitation flux for the event in a) Feb 1980, b) Feb-Mar 1991, c) Jan 1993, d) Jan 2008, e) Jan 2010 for all sets of simulations

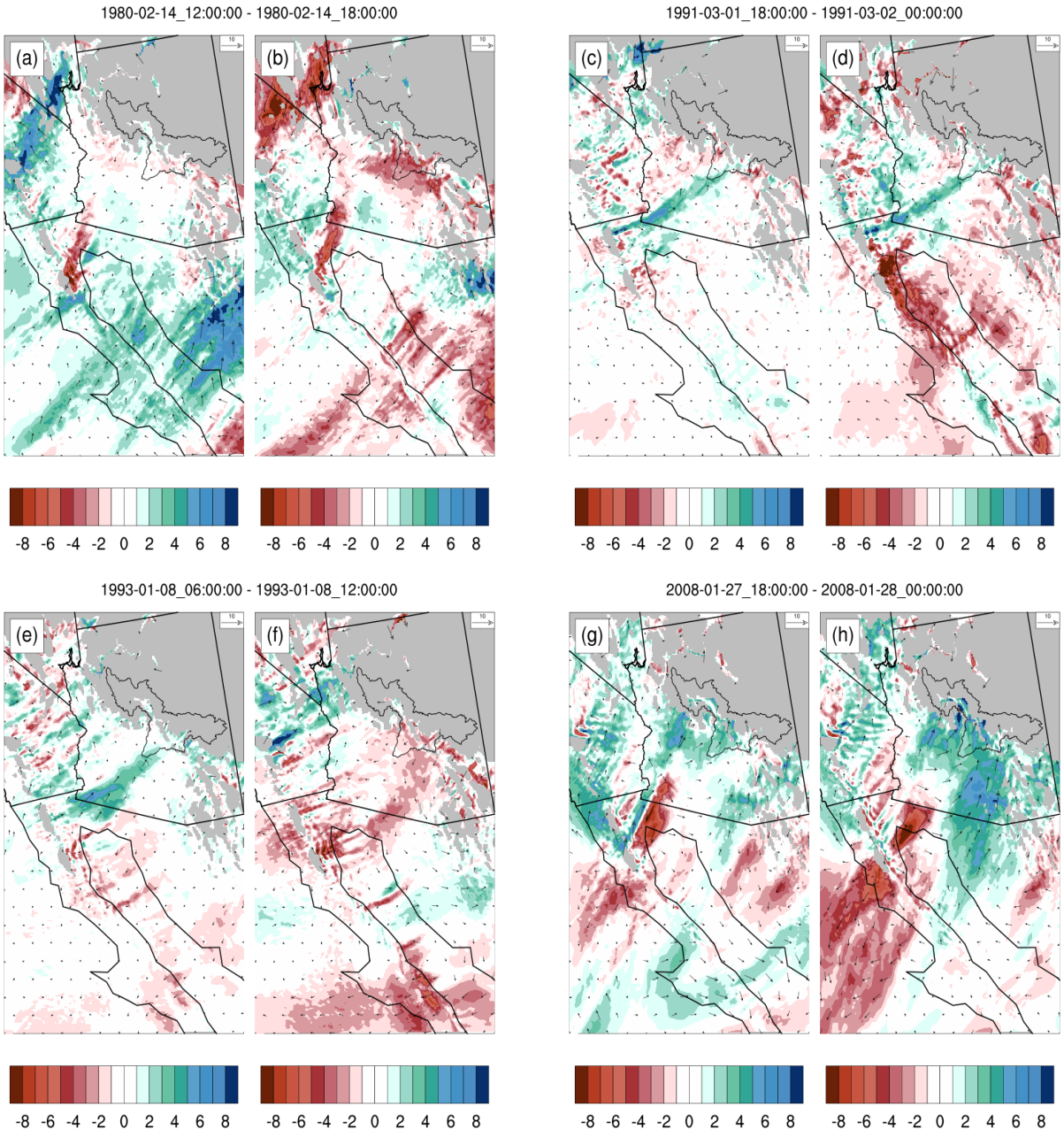

Figure 10 Difference between future and control 850 mb speed (ms^{-1}; shaded) for PGW1 (left) and PGW2 (right) simulations averaged over (a),(b) 14 Jan 1980 1200 -1800UTC (c),(d) 1 Mar 1991 1800UTC – 2 Mar 1991 0000UTC (e),(f) 8 Jan 1993 0600 – 1200 UTC (g),(h) 27 Jan 2008 1800 UTC – 28 Jan 2008 0000 UTC (i),(j) 22 Jan 2010 0000 - 0600 UTC. The difference vectors are also shown. The reference vector is shown on the top right corner.

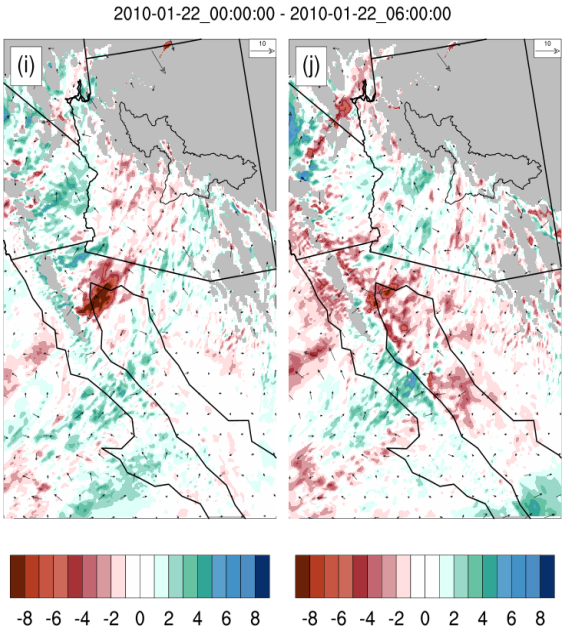

Figure 10 (cont.)

REFERENCES

Bryson, R. A., and F. K. Hare (1974), The Climates of North America, in *Climates of North America*, vol. 11, pp. 1–47.

Dacre, H. F., P. A. Clark, O. Martinez-Alvarado, M. A. Stringer, and D. A. Lavers (2014), How Do Atmospheric Rivers Form?, *Bull. Am. Meteorol. Soc.*, *96*(8), 1243–1255, doi:10.1175/BAMS-D-14-00031.1.

Dee, D. P. et al. (2011), The ERA-Interim reanalysis: configuration and performance of the data assimilation system, *Q. J. R. Meteorol. Soc.*, *137*(656), 553–597, doi:10.1002/qj.828.

Dettinger, M. (2011), Climate Change, Atmospheric Rivers, and Floods in California - A Multimodel Analysis of Storm Frequency and Magnitude Changes1, *JAWRA J. Am. Water Resour. Assoc.*, *47*(3), 514–523, doi:10.1111/j.1752-1688.2011.00546.x.

Dettinger, M. D., F. M. Ralph, T. Das, P. J. Neiman, and D. R. Cayan (2011), Atmospheric Rivers, Floods and the Water Resources of California, *Water*, *3*(4), 445–478, doi:10.3390/w3020445.

Diffenbaugh, N. S., J. S. Pal, R. J. Trapp, and F. Giorgi (2005), Fine-scale processes regulate the response of extreme events to global climate change, *Proc. Natl. Acad. Sci.*, *102*(44), 15774–15778, doi:10.1073/pnas.0506042102.

Donner, L. J. et al. (2011), The Dynamical Core, Physical Parameterizations, and Basic Simulation Characteristics of the Atmospheric Component AM3 of the GFDL Global Coupled Model CM3, *J. Clim.*, *24*(13), 3484–3519, doi:10.1175/2011JCLI3955.1.

Dufresne, J. L. et al. (2013), Climate change projections using the IPSL-CM5 Earth System Model: From CMIP3 to CMIP5, *Clim. Dyn.*, *40*(9–10), 2123–2165, doi:10.1007/s00382-012-1636-1.

Emori, S. (2005), Dynamic and thermodynamic changes in mean and extreme precipitation under changed climate, *Geophys. Res. Lett.*, *32*(17), L17706, doi:10.1029/2005GL023272.

Gao, Y., J. Lu, L. R. Leung, Q. Yang, S. Hagos, and Y. Qian (2015), Dynamical and thermodynamical modulations on future changes of landfalling atmospheric rivers over western North America, *Geophys. Res. Lett.*, *42*(17), 7179–7186, doi:10.1002/2015GL065435.

Gent, P. R. et al. (2011), The community climate system model version 4, *J. Clim.*, *24*(19), 4973–4991, doi:10.1175/2011JCLI4083.1.

Hagos, S. M., L. R. Leung, J. H. Yoon, J. Lu, and Y. Gao (2016), A projection of changes in landfalling atmospheric river frequency and extreme precipitation over western North America from the Large Ensemble CESM simulations, *Geophys. Res. Lett.*, *43*(3), 1357–1363, doi:10.1002/2015GL067392.

Hazeleger, W., B. J. J. M. van den Hurk, E. Min, G. J. van Oldenborgh, A. C. Petersen, D. A. Stainforth, E. Vasileiadou, and L. A. Smith (2015), Tales of future weather, *Nat. Clim. Chang.*, *5*(2), 107–113, doi:10.1038/nclimate2450.

Hong, S.-Y., Y. Noh, and J. Dudhia (2006), A New Vertical Diffusion Package with an Explicit Treatment of Entrainment Processes, *Mon. Weather Rev.*, *134*(9), 2318–2341, doi:10.1175/MWR3199.1.

Hughes, M., K. M. Mahoney, and P. J. Neiman (2014), The landfall and inland penetration of a flood-producing atmospheric river in Arizona. Part II: Sensitivity of modeled precipitation to terrain height and atmospheric river …, *J.* ….

Iacono, M. J., J. S. Delamere, E. J. Mlawer, M. W. Shephard, S. A. Clough, and W. D. Collins (2008), Radiative forcing by long-lived greenhouse gases: Calculations with the AER radiative transfer models, *J. Geophys. Res.*, *113*(D13), D13103, doi:10.1029/2008JD009944.

Jones, C. D. et al. (2011), The HadGEM2-ES implementation of CMIP5 centennial simulations, *Geosci. Model Dev.*, *4*(3), 543–570, doi:10.5194/gmd-4-543-2011.

Kain, J. S. (2004), The Kain–Fritsch Convective Parameterization: An Update, *J. Appl. Meteorol.*, *43*(1), 170–181.

Kawase, H., T. Yoshikane, M. Hara, F. Kimura, T. Yasunari, B. Ailikun, H. Ueda, and T. Inoue (2009), Intermodel variability of future changes in the Baiu rainband estimated by the pseudo global warming downscaling method, *J. Geophys. Res. Atmos.*, *114*(24), doi:10.1029/2009JD011803.

Knippertz, P., and J. E. Martin (2007), A Pacific Moisture Conveyor Belt and Its Relationship to a Significant Precipitation Event in the Semiarid Southwestern United States, *Weather Forecast.*, *22*(1), 125–144, doi:10.1175/WAF963.1.

Lackmann, G. M. (2002), Cold-Frontal Potential Vorticity Maxima, the Low-Level Jet, and Moisture Transport in Extratropical Cyclones, *Mon. Weather Rev.*, *130*(1), 59–74, doi:10.1175/1520-0493(2002)130<0059:CFPVMT>2.0.CO;2.

Lackmann, G. M. (2013), The south-central U.S. flood of may 2010: Present and future, *J. Clim.*, *26*(13), 4688–4709, doi:10.1175/JCLI-D-12-00392.1.

Lackmann, G. M. (2015), Hurricane Sandy before 1900 and after 2100, *Bull. Am. Meteorol. …*.

Lauer, A., C. Zhang, E.-T. Oliver, Y. Wang, and K. Hamilton (2013), Downscaling of Climate Change in the Hawaii Region Using {CMIP5} Results: On the Choice of the Forcing Fields*, *J Clim.*, *26*(24), 10006–10030, doi:10.1175/JCLI-D-13-00126.1.

Lavers, D. a, R. P. Allan, G. Villarini, B. Lloyd-Hughes, D. J. Brayshaw, and A. J. Wade (2013), Future changes in atmospheric rivers and their implications for winter flooding in Britain, *Environ. Res. Lett.*, *8*, 34010, doi:10.1088/1748-9326/8/3/034010.

Lavers, D. A., R. P. Allan, E. F. Wood, G. Villarini, D. J. Brayshaw, and A. J. Wade (2011), Winter floods in Britain are connected to atmospheric rivers, *Geophys. Res. Lett.*, *38*(23), n/a-n/a, doi:10.1029/2011GL049783.

Lavers, D. A., G. Villarini, R. P. Allan, E. F. Wood, and A. J. Wade (2012), The detection of atmospheric rivers in atmospheric reanalyses and their links to British winter floods and the large-scale climatic circulation, *J. Geophys. Res. Atmos.*, *117*(20), doi:10.1029/2012JD018027.

Lenderink, G., and E. van Meijgaard (2008), Increase in hourly precipitation extremes beyond expectations from temperature changes, *Nat. Geosci.*, *1*(8), 511–514, doi:10.1038/ngeo262.

Leung, L. R., and Y. Qian (2009), Atmospheric rivers induced heavy precipitation and flooding in the western U.S. simulated by the WRF regional climate model, *Geophys. Res. Lett.*, *36*(3), L03820, doi:10.1029/2008GL036445.

Leung, L. R., Y. Qian, X. Bian, W. M. Washington, J. Han, and J. O. Roads (2004), Mid-century ensemble regional climate change scenarios for the western United States, *Clim. Change*, *62*(1–3), 75–113, doi:10.1023/B:CLIM.0000013692.50640.55.

Livneh, B., E. A. Rosenberg, C. Lin, B. Nijssen, V. Mishra, K. M. Andreadis, E. P. Maurer, and D. P. Lettenmaier (2013), A Long-Term Hydrologically Based Dataset of Land Surface Fluxes and States for the Conterminous United States: Update and Extensions*, *J. Clim.*, *26*(23), 9384–9392, doi:10.1175/JCLI-D-12-00508.1.

Lynn, B., R. Healy, and L. Druyan (2009), Investigation of Hurricane Katrina characteristics for future, warmer climates, *Clim. Res.*, *39*(1), 75–86, doi:10.3354/cr00801.

Mearns, L. O., W. Gutowski, R. Jones, R. Leung, S. McGinnis, A. Nunes, and Y. Qian (2009), A Regional Climate Change Assessment Program for North America, *Eos, Trans. Am. Geophys. Union*, *90*(36), 311–311, doi:10.1029/2009EO360002.

Miguez-Macho, G., G. L. Stenchikov, and A. Robock (2004), Spectral nudging to eliminate the effects of domain position and geometry in regional climate model simulations, *J. Geophys. Res. D Atmos.*, *109*(13), doi:10.1029/2003JD004495.

Morrison, H., G. Thompson, and V. Tatarskii (2009), Impact of Cloud Microphysics on the Development of Trailing Stratiform Precipitation in a Simulated Squall Line: Comparison of One- and Two-Moment Schemes, *Mon. Weather Rev.*, *137*(3), 991–1007, doi:10.1175/2008MWR2556.1.

Mote, P. W. (2003), Trends in snow water equivalent in the Pacific Northwest and their climatic causes, *Geophys. Res. Lett.*, *30(12)*(L1601), 1–4, doi:10.1029/2003GL017258.

Neiman, P. J., F. M. Ralph, G. A. Wick, Y.-H. Kuo, T.-K. Wee, Z. Ma, G. H. Taylor, and M. D. Dettinger (2008a), Diagnosis of an Intense Atmospheric River Impacting the Pacific Northwest: Storm Summary and Offshore Vertical Structure Observed with COSMIC Satellite Retrievals, *Mon. Weather Rev.*, *136*(11), 4398–4420, doi:10.1175/2008MWR2550.1.

Neiman, P. J., F. M. Ralph, G. A. Wick, J. D. Lundquist, and M. D. Dettinger (2008b), Meteorological Characteristics and Overland Precipitation Impacts of Atmospheric Rivers Affecting the West Coast of North America Based on Eight Years of SSM/I Satellite Observations, *J. Hydrometeorol.*, *9*(1), 22–47, doi:10.1175/2007JHM855.1.

Neiman, P. J., L. J. Schick, F. M. Ralph, M. Hughes, and G. A. Wick (2011a), Flooding in Western Washington: The Connection to Atmospheric Rivers*, *J. Hydrometeorol.*, *12*(6), 1337–1358, doi:10.1175/2011JHM1358.1.

Neiman, P. J., L. J. Schick, F. M. Ralph, M. Hughes, and G. a. Wick (2011b), Flooding in Western Washington: The Connection to Atmospheric Rivers*, *J. Hydrometeorol.*, *12*(6), 1337–1358, doi:10.1175/2011JHM1358.1.

Neiman, P. J., F. M. Ralph, and B. J. Moore (2013), The landfall and inland penetration of a flood-producing atmospheric river in Arizona. Part I: Observed synoptic-scale, orographic, and hydrometeorological …, *J.* ….

Pall, P., M. R. Allen, and D. A. Stone (2007), Testing the Clausius–Clapeyron constraint on changes in extreme precipitation under CO2 warming, *Clim. Dyn.*, *28*(4), 351–363, doi:10.1007/s00382-006-0180-2.

Payne, A. E., and G. Magnusdottir (2015), An evaluation of atmospheric rivers over the North Pacific in CMIP5 and their response to warming under RCP 8.5, *J. Geophys. Res. Atmos.*, *120*(21), 11,111-173,190, doi:10.1002/2015JD023586.

Ralph, F. M., P. J. Neiman, G. A. Wick, S. I. Gutman, M. D. Dettinger, D. R. Cayan, and A. B. White (2006), Flooding on California's Russian River: Role of atmospheric rivers, *Geophys. Res. Lett.*, *33*(13), L13801, doi:10.1029/2006GL026689.

Rasmussen, R. et al. (2011), High-Resolution Coupled Climate Runoff Simulations of Seasonal Snowfall over Colorado: A Process Study of Current and Warmer Climate, *J. Clim.*, *24*(12), 3015–3048, doi:10.1175/2010JCLI3985.1.

Rienecker, M. M. et al. (2011), MERRA: NASA's Modern-Era Retrospective Analysis for Research and Applications, *J. Clim.*, *24*(14), 3624–3648, doi:10.1175/JCLI-D-11-00015.1.

Rivera, E. R., and F. Dominguez (2016), Projected changes in atmospheric river events in Arizona as simulated by global and regional climate models, *Clim. Dyn.*, *47*(5–6), 1673–1691, doi:10.1007/s00382-015-2927-0.

Rivera, E. R., F. Dominguez, and C. L. Castro (2013), Atmospheric Rivers and Cool Season Extreme Precipitation Events in the Verde River Basin of Arizona, *J. Hydrometeorol.*, *15*(2), 813–829, doi:10.1175/JHM-D-12-0189.1.

Rivera, E. R., F. Dominguez, and C. L. Castro (2014), Atmospheric Rivers and Cool Season Extreme Precipitation Events in the Verde River Basin of Arizona TL - 15, *J. Hydrometeorol.*, *15 VN-r*(2), 813–829, doi:10.1175/JHM-D-12-0189.1.

Rutz, J. J., and W. J. Steenburgh (2012), Quantifying the role of atmospheric rivers in the interior

western United States, *Atmos. Sci. Lett.*, *13*(4), 257–261, doi:10.1002/asl.392.

Rutz, J. J., W. J. Steenburgh, and F. M. Ralph (2014), Climatological characteristics of atmospheric rivers and their inland penetration over the western United States, *Mon. Weather Rev.*, *142*(February 2006), 905–921, doi:10.1175/MWR-D-13-00168.1.

Rutz, J. J., W. J. Steenburgh, and F. M. Ralph (2015), The inland penetration of atmospheric rivers over western north america: A lagrangian analysis, *Mon. Weather Rev.*

Sato, T., F. Kimura, and A. Kitoh (2007), Projection of global warming onto regional precipitation over Mongolia using a regional climate model, *J. Hydrol.*, *333*(1), 144–154, doi:10.1016/j.jhydrol.2006.07.023.

Schär, C., C. Frei, D. Lüthi, and H. C. Davies (1996a), Surrogate climate-change scenarios for regional climate models, *Geophys. Res. Lett.*, *23*(6), 669–672, doi:10.1029/96GL00265.

Schär, C., C. Frei, D. Lüthi, and H. C. Davies (1996b), Surrogate climate change scenarios for regional climate models TL - 23, *Geophys. Res. Lett.*, *23 VN*(6), 669–672, doi:10.1029/96GL00265.

Sheppard, P. R., A. C. Comrie, G. D. Packin, K. Angersbach, and M. K. Hughes (2002), The climate of the US Southwest, *Clim. Res.*, *21*(3), 219–238, doi:10.3354/cr021219.

Shi, X., and D. Durran (2016), Sensitivities of Extreme Precipitation to Global Warming Are Lower over Mountains than over Oceans and Plains, *J. Clim.*, *29*(13), 4779–4791, doi:10.1175/JCLI-D-15-0576.1.

Siler, N., and G. Roe (2014), How will orographic precipitation respond to surface warming? An idealized thermodynamic perspective, *Geophys. Res. Lett.*, *41*(7), 2606–2613,

doi:10.1002/2013GL059095.

Skamarock, W. C., J. B. Klemp, J. Dudhi, D. O. Gill, D. M. Barker, M. G. Duda, X.-Y. Huang, W. Wang, and J. G. Powers (2008), *A Description of the Advanced Research WRF Version 3*.

Stainforth, D. ., M. . Allen, E. . Tredger, and L. . Smith (2007), Confidence, uncertainty and decision-support relevance in climate predictions, *Philos. Trans. R. Soc. A Math. Phys. Eng. Sci.*, *365*(1857), 2145–2161, doi:10.1098/rsta.2007.2074.

Stohl, A., C. Forster, and H. Sodemann (2008), Remote sources of water vapor forming precipitation on the Norwegian west coast at 60°N-a tale of hurricanes and an atmospheric river, *J. Geophys. Res. Atmos.*, *113*(D5), n/a-n/a, doi:10.1029/2007JD009006.

Tewari, M., F. Chen, W. Wang, J. Dudhia, M. A. LeMone, K. Mitchell, M. Ek, G. Gayno, J. Wegiel, and R. H. Cuenca (2004), Implementation and verification of the unified NOAH land surface model in the WRF model, in *20th Conference on Weather Analysis and Forecasting/16th Conference on Numerical Weather Prediction*, pp. 11–15.

Trenberth, K. E. (1999), Conceptual framework for changes of extremes of the hydrological cycle with climate change, *Clim. Change*, *42*(1), 327–339, doi:10.1023/A:1005488920935.

Trenberth, K. E., A. Dai, R. M. Rasmussen, and D. B. Parsons (2003), The changing character of precipitation, *Bull. Am. Meteorol. Soc.*, *84*(9), 1205–1217+1161, doi:10.1175/BAMS-84-9-1205.

van Vuuren, D. P. et al. (2011), The representative concentration pathways: An overview, *Clim. Change*, *109*(1), 5–31, doi:10.1007/s10584-011-0148-z.

Wasko, C., A. Sharma, and F. Johnson (2015), Does storm duration modulate the extreme precipitation-temperature scaling relationship?, *Geophys. Res. Lett.*, *42*(20), 8783–8790, doi:10.1002/2015GL066274.

Watanabe, M. et al. (2010), Improved climate simulation by MIROC5: Mean states, variability, and climate sensitivity, *J. Clim.*, *23*(23), 6312–6335, doi:10.1175/2010JCLI3679.1.

Xiao-Ge, X., W. Tong-Wen, and Z. Jie (2013), Introduction of CMIP5 Experiments Carried out with the Climate System Models of Beijing Climate Center, *Adv. Clim. Chang. Res.*, *4*(1), 41–49, doi:10.3724/SP.J.1248.2013.041.

Zhang, Z. S., K. Nisancioglu, M. Bentsen, J. Tjiputra, I. Bethke, Q. Yan, B. Risebrobakken, C. Andersson, and E. Jansen (2012), Pre-industrial and mid-Pliocene simulations with NorESM-L, *Geosci. Model Dev.*, *5*(2), 523–533, doi:10.5194/gmd-5-523-2012.

Zhu, Y., and R. E. Newell (1998), A Proposed Algorithm for Moisture Fluxes from Atmospheric Rivers, *Mon. Weather Rev.*, *126*(3), 725–735, doi:10.1175/1520-0493(1998)126<0725:APAFMF>2.0.CO;2.